Proceedings of ALGORITMY 2012
pp. 53–64

INTERFACE PROBLEMS FOR QUASI-LINEAR ELLIPTIC EQUATIONS BY MATERIAL AND SHAPE DERIVATIVE METHODS*

IVAN CIMRÁK†

Abstract. A shape determinaton problem is studied for quasilinear elliptic problems. Such problems describe interface problems. The ultimate goal of our research is to determine the interface between two materials with different physical properties. The interface is identified by the minimization of the shape (or the cost) functional evaluating the misfit between the data and the simulations.

We elaborate the material and shape derivative method. We characterize the elliptic interface problems whose solutions give the material and shape derivatives. Further we employ the adjoint variable method to obtain an explicit expression for the gradient of the shape functional.

For the representation of the interface we use the level set method. Simulation presented show the reconstruction of voids in a nonlinear ferromagnetic material. Available data are measurements of magnetic induction.

Key words. sensitivity analysis, shape derivative, material derivative, adjoint problem, shape optimization, level set method

AMS subject classifications. 65M32, 49Q12

1. Introduction. Defect characterization in magnetic materials uses local magnetic measurements. A hard magnetic workpiece made of a nonlinear magnetic material is put in a magnetic field generated by some source. Non-linearity of the material is represented by a strongly nonlinear magnetic reluctivity $\beta(\mathbf{x}, |\mathbf{B}|^2)$ (often denoted also by ν) that depends not only on the position vector $\mathbf{x}$ but also on the strength of the magnetic induction. Small inhomogeneities can occur during the steel production process, such as small air gaps or cracks inside a workpiece. The magnetic reluctivity of the air is significantly different as that of the nonlinear magnetic material. Therefore the magnetic reluctivity $\beta(\mathbf{x}, |\mathbf{B}|^2)$ defined over the whole domain has discontinuities over the borders of the air gaps or cracks. Once these discontinuities are located, one has also the position and the shape of actual air gaps or cracks.

Governing equations are derived from the static distribution of the magnetic field under the induced current with the current density f. Equations are written in the magnetic vector potential formulation of the static Maxwell equations. We consider the planar symmetry with the symmetry plane xy. The only non-zero component of the vector potential is denoted by u. In this formulation with planar symmetry, the magnetic induction has two non-zero components and can be expressed as $\left(\frac{\partial u}{\partial y}, -\frac{\partial u}{\partial x}, 0\right)^{\mathrm{T}}$. This reduces the three-dimensional case to the 2D case. Suppose that the magnetic potential vanishes on the boundary. Then u satisfies the following quasi-linear problem:

$$-\nabla \cdot \big(\beta(\mathbf{x}, |\nabla u|^2)\nabla u\big) = f(\mathbf{x}) \quad \text{in } D, \qquad u = 0 \quad \text{on } \partial D, \tag{1.1}$$

*The research leading to these results has received funding from the People Programme (Marie Curie Actions) of the European Union's Seventh Framework Programme (FP7/2007-2013) under REA grant agreement no. PCIG10-GA-2011-303580

†Department of Software Technologies, Faculty of Management Sciences and Informatics, University of Žilina, Univerzitná 8215/1, 010 26, Žilina, Slovakia (ivan.cimrak@fri.uniza.sk).

with the following interface conditions

$$\big[u\big]\Big|_{\partial\Omega} = 0, \qquad \big[\beta(\mathbf{x}, |\nabla u|^2)\nabla u \cdot \mathbf{n}\big]\Big|_{\partial\Omega} = 0, \tag{1.2}$$

where $\big[v\big]$ is the jump of a quantity v across the interface $\partial\Omega$ and $\mathbf{n}$ the unit outward normal to the boundary $\partial\Omega$. In above, D is a bounded domain in $\mathbb{R}^2$ with C^2 boundary and $\Omega \subset D$ its proper subdomain with C^2 boundary. Assume that the function $\beta : D \times \mathbb{R} \to \mathbb{R}$ is defined piecewise by

$$\beta(\mathbf{x}, s) = \begin{cases} \beta_1(s) & \text{for } \mathbf{x} \in \Omega, \\ \beta_2(s) & \text{for } \mathbf{x} \in D \setminus \Omega, \end{cases} \tag{1.3}$$

where β_1, β_2 are smooth nonlinear functions. Further we assume that the functions $s \to \beta_i(s)$ are non-decreasing, there exists positive β_{min} such that $\beta_i(s) \geq \beta_{min}$, there exists positive β_{max} such that $\beta_i(s) \leq \beta_{max}$, and both β_i are differentiable with well-defined derivatives β_i' satisfying $\beta_i' \leq \beta_{max}'$. These assumptions create the monotonicity structure of the differential operator, and they guarantee that the equation (1.4) does not degenerate. Also, we assume $f, \nabla f \in L^\infty(D)$.

For linear materials, the reluctivity is a scalar function leading to a simpler linear elliptic PDE. Such linear system describes the problem of EIT which has been thoroughly studied by many authors, see [1] and the references therein. Also, when β does not depend on ∇u and depends on u, the resulting equation governs the problem of inverse thermal imaging. We tackled this problem in [3].

The ultimate goal of this work is the reconstruction of Ω if we possess the values of ∇u on D. We point out that such an inverse problem for quasi-linear state equations has not yet been studied. Its linear version has been studied in [9].

Direct problem. The direct problem can be formulated in a weak sense: Find $u \in W_0^{1,2}(D)$ such that

$$\big(\beta(|\nabla u|^2)\nabla u, \nabla\varphi\big) = \big(f, \varphi\big), \tag{1.4}$$

is satisfied for all $\varphi \in W_0^{1,2}(D)$.

According to the theoretical analysis of the direct problem from [13] and [16] we can conclude existence and uniqueness of solutions u with the following regularity:

$$u \in C^{1,\alpha}(\overline{D}), \quad u\Big|_{\Omega} \in C^{2,\alpha}(\Omega), \quad u\Big|_{D\setminus\overline{\Omega}} \in C^{2,\alpha}(D \setminus \overline{\Omega}).$$

We are interested in the reconstruction of Ω for given β_1, β_2 and given data on D corresponding to ∇u. We seek Ω, such that the gradient of the state variable ∇u is as close as possible to the data, that is ∇u fits the vector field $\mathbf{B}$. To measure the misfit we construct a cost functional

$$J(\Omega) = \frac{1}{2}\int_D |\nabla u(\Omega) - \mathbf{B}|^2 \tag{1.5}$$

where for given Ω, $u(\Omega)$ is the solution to (1.4). We formalize the definition of the inverse problem:

Inverse problem. Find the shape Ω minimizing $J(\Omega)$, i.e. find Ω_{opt} such that $\Omega_{opt} = \arg\min_\Omega J(\Omega)$. To achieve this goal we use a gradient-type minimization method to minimize the cost function. Such methods need to compute the gradient

DJ of J. We employ the shape sensitivity analysis using the material and the shape derivative as tools for computation of DJ.

We have solved similar problem in [6]. There, we have minimized the cost functional $J(\Omega)$ using the Gâteaux derivative of $J(\Omega)$. However, the explicit form of the Gâteaux derivative was obtained only formally.

Here we use different approach. The shape and material derivative has been widely used in the shape optimization, see e.g. [2, 8, 15, 17] and the references therein. This concept has been applied in the shape sensitivity for unilateral problems describing such physical phenomena as contact problems in elasticity, elasto-plastic torsion problems, obstacle problems and others.

We point out that the transition from the linear elliptic state equation treated in [10] to the quasi-linear case is not trivial.

2. Material and shape derivative method. The overview of material derivative method can be found in [15]. We introduce basic concepts and notation including the notion of the solution to the direct problem in a time instance t denoted by u^t. Then we state the equation that is satisfied by $w^t = (u^t - u)/t$, together with the weak convergence. We state the explicit formula for the weak material derivative denoted by $\dot{u}$. We make a remark on the strong convergence.

We use an artificial time variable t. Domain Ω evolves in time for $t > 0$. We denote by Ω_t the evolved Ω in the time instance t. At every time instance t we can formulate the direct problem in the weak formulation

$$(\beta_t(|\nabla u_t|^2)\nabla u_t, \nabla\varphi_t) = (f, \varphi_t). \tag{2.1}$$

The nonlinearity is defined as

$$\beta_t(\mathbf{x}, s) = \begin{cases} \beta_1(s) & \text{for } \mathbf{x} \in \Omega_t, \\ \beta_2(s) & \text{for } \mathbf{x} \in D \setminus \Omega_t. \end{cases} \tag{2.2}$$

The cost functional is then written as

$$J(\Omega_t) = \frac{1}{2}\int_D |\nabla u_t - \mathbf{B}|^2. \tag{2.3}$$

For the velocity field we use symbol $\mathbf{h}(\mathbf{x})$. We look what is the response of J onto small movement of Ω in the direction of this velocity field. Performing such sensitivity analysis we will be able to determine the correct $\mathbf{h}$ under which Ω must be moved to decrease the value of J.

For non-negative $t \in \mathbb{R}$ define the mapping $F_t : \mathbb{R}^2 \to \mathbb{R}^2$ by

$$F_t(\mathbf{X}) = \mathbf{X} + t\mathbf{h}(\mathbf{X}), \tag{2.4}$$

where $\mathbf{h}(\mathbf{X}) = (h_1(\mathbf{X}), h_2(\mathbf{X}))^T \in (C^{1,1}(\mathbb{R}^2))^2$ and $\mathbf{h} = \mathbf{0}$ on ∂D. For t sufficiently small let $\Omega_t = F_t(\Omega)$ be the image of the fixed domain Ω. Since $F_t|_{t=0} = Id$ we have $\Omega_0 = \Omega$. We use symbol $\mathbf{X}$ for the points in $\mathbb{R}^2$ where $\mathbb{R}^2$ is considered as the definition domain of F_t. We use $\mathbf{x}$ for points in $\mathbb{R}^2$ where $\mathbb{R}^2$ is considered as the range of F_t. F_t is considered as the mapping from the fixed frame to the moving frame. The moving frame moves under the velocity field $\mathbf{h}$. By writing a symbol D in front of a vector function $\mathbf{f}$ we mean the matrix

$$D\mathbf{f} = \begin{pmatrix} \frac{\partial f_1}{\partial x_1} & \frac{\partial f_1}{\partial x_2} \\ \\ \frac{\partial f_2}{\partial x_1} & \frac{\partial f_2}{\partial x_2} \end{pmatrix}.$$

Denote $M_t = (DF_t)^{-1}$, $I_t = \det(DF_t)$, $A_t := M_t M_t^T I_t$ and $A := \nabla\cdot\mathbf{h}Id - (D\mathbf{h}^T + D\mathbf{h})$.

The functions depending on $\mathbf{X}$ (i.e. those with domain in the fixed frame) will be marked by superscript t and functions depending on $\mathbf{x}$ (i.e. those with domain in moving frame) will be marked by subscript t. Thus

$$u^t(\mathbf{X}) = u_t(\mathbf{x}) = u_t(F_t(\mathbf{X})), \quad \text{or} \quad u^t = u_t \circ F_t.$$

Since $(M_t^T)^{-1} = (M_t^{-1})^T$ we have the following

$$\nabla u^t = DF^T(\nabla u_t) \circ F_t, \quad M_t^T(\nabla u^t) \circ F_t^{-1} = \nabla u_t. \tag{2.5}$$

The material derivative is defined as $\dot{u} = \lim_{t\to 0} \frac{u^t - u}{t}$. We derive the equation for $w^t := (u^t - u)/t$ and then we pass in the limit for $t \to 0$ to obtain an equation for $\dot{u}$. Such derivation is nontrivial and rather technical and will be published elsewhere. The outcome of such procedure is that $w^t \rightharpoonup \dot{u}$ in $W^{1,2}(D)$ and $\dot{u}$ satisfies the following equation for the weak material derivative

$$\begin{aligned}&(\beta(|\nabla u|^2)\nabla\dot{u}, \nabla\varphi) + 2(\beta'(|\nabla u|^2)\nabla\dot{u}\cdot\nabla u\nabla u, \nabla\varphi) \\ &+(\beta(|\nabla u|^2)A\nabla u, \nabla\varphi) + 2(\beta'(|\nabla u|^2)(-D\mathbf{h}^T)\nabla u\cdot\nabla u\nabla u, \nabla\varphi) + (-\nabla\cdot(f\mathbf{h}), \varphi) = 0,\end{aligned} \tag{2.6}$$

where the equality is satisfied for all $\varphi \in W^{1,2}(D)$. It is also possible to show strong convergence $w^t \to \dot{u}$ strongly in $W^{1,2}(D)$. This result will be published elsewhere.

Using stronger assumption on the regularity of u one can derive an explicit expression for the shape derivative. Recall that the shape derivative of u is a function defined by

$$u' = \dot{u} - \mathbf{h}\cdot\nabla u.$$

Assuming that the solution u to the direct problem (1.1),(1.2) satisfy $u \in W^{2,2}(\Omega)$, and $u \in W^{2,2}(D\setminus\overline{\Omega})$, one can show that the shape derivative u' satisfies the following elliptic interface problem

$$(\beta(|\nabla u|^2)\nabla u', \nabla\varphi) + 2(\beta'(|\nabla u|^2)\nabla u'\cdot\nabla u\nabla u, \nabla\varphi) = (\mathbf{h}\cdot\mathbf{n}_\Omega(Pu^+ - Pu^-), \nabla\varphi)_{\partial\Omega}. \tag{2.7}$$

Again, technical details of the proof will be presented elsewhere.

3. Adjoint problem. Minimization procedures follow direction of the descent. To find them, one needs to know the response of the cost functional on the small changes of Ω under the velocity field induced by F_t. We differentiate the cost function (2.3)

$$DJ := \lim_{t\to 0}\frac{J(\Omega_t) - J(\Omega)}{t} = \lim_{t\to 0}\frac{1}{2t}\left[\int_D |\nabla u_t - \mathbf{B}|^2 - |\nabla u - \mathbf{B}|^2\right] = \int_D (\nabla u - \mathbf{B})\cdot\nabla u'. \tag{3.1}$$

using results from [10, 15].

We introduce an adjoint problem in order to explicitly compute the derivative of the cost function $J(\Omega)$. This reduces computational costs tremendously in comparison with the conventional method of perturbations or with the method of sensitivity equation. This speed up is caused by the fact that the direct problem is nonlinear and therefore it must be solved iteratively. A similar approach of an adjoint variable has been used in many applications [5, 4, 7, 12, 14].

By p denote a function such that $p \in W_0^{2,2}(D)$ and for all $\psi \in W_0^{2,2}(D)$

$$(\beta(|\nabla u|^2)\nabla p, \nabla\psi) + 2(\beta'(|\nabla u|^2)\nabla p \cdot \nabla u \nabla u, \nabla\psi) = \int_\omega (\nabla u - \mathbf{B}) \cdot \nabla\psi. \tag{3.2}$$

Take the following test functions $\varphi = p$ in (2.7) and $\psi = u'$ in (3.2). The left-hand sides of the resulting equalities are equal and therefore we obtain

$$DJ = \int_D (\nabla u - \mathbf{B}) \cdot \nabla u' = (\mathbf{h} \cdot \mathbf{n}_\Omega (Pu^+ - Pu^-), \nabla p)_{\partial\Omega}. \tag{3.3}$$

Thus, the steepest descent direction (denoted by $\mathbf{h}_{sd}$) for the gradient-type algorithms minimizing J is given by

$$\mathbf{h}_{sd} = -(Pu^+ - Pu^-) \cdot \nabla p \mathbf{n}_\Omega, \qquad \text{on } \partial\Omega. \tag{3.4}$$

4. Implementation. We use the level set method [10, 11]. We represent the boundary of Ω as a zero level set of a function ϕ. We set ϕ in such a manner that $\Omega = \{\mathbf{x} \in D \mid \phi(\mathbf{x}) > 0\}$, $D \setminus \Omega = \{\mathbf{x} \in D \mid \phi(\mathbf{x}) < 0\}$. For computations we take the approximation of the Heaviside function

$$H_k(\phi) = \frac{1}{2} + \frac{1}{\pi} \arctan(k\phi),$$

with a real parameter k, influencing how steep is the approximation around zero. For $k \to \infty$, $H_k(\phi)$ converges point wise to $H(\phi)$.

Minimization of the shape functional J is done by moving the interface $\partial\Omega$ in the steepest descent direction $\mathbf{h}_{sd}$. The level set method allows us to do this by solving the Hamilton-Jacobi equation.

Given data on the domain ω, the following algorithm identifies the unknown Ω inside the domain D.

ALGORITHM 1.

(a) **Set** *an initial level set function ϕ as an initial guess. By j we indicate the quantities in the jth step of this algorithm.* **For** *$j = 0, j = 1, \ldots,$ do the following until the algorithm converges.*

(b) **Solve** *(1.4) with Ω_j instead of Ω to obtain the solution u_j of the direct problem.*

(c) **Solve** *(3.2) with Ω_j and u_j instead of Ω and u to obtain the solution p_j of the adjoint problem.*

(d) **Evaluate** *the normal steepest descent direction h_{sd}^j from (3.4).*

(e) **Update** *the level set function by solving the Hamilton-Jacobi equation.*

(f) **If** *the convergence is reached* **then** *stop* **otherwise** *shift the index j with the corresponding quantities and go to the (b) part of this algorithm.*

The Hamilton–Jacobi equation [11] solved in part (e) has the form $\phi_t + \mathbf{h}_{sd} \cdot \nabla\phi = 0$. For its discretization we use the scheme

$$\frac{\phi^{j+1} - \phi^j}{\Delta t} + h_{sd}^j |\nabla\phi^j| = 0.$$

Throughout this section we consider $\Omega \in \mathbb{R}^2$ to be a square $(-0.5, 0.5) \times (-0.5, 0.5)$. The material parameter functions β_1, β_2 are set to conform the real physical quantities as described in the Introduction. $\beta_1 = 7.961 \times 10^5$ which is a constant equal to

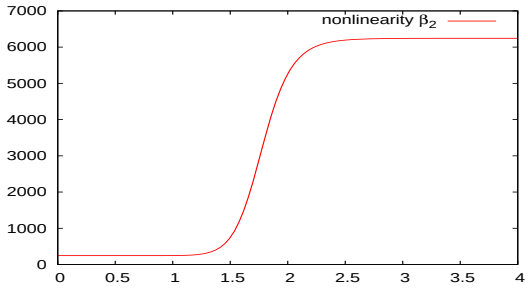

FIG. 4.1. *Non-linear function* $\beta_2(s)$.

the inverse of the magnetic permeability of the air. β_2 is chosen to be

$$\beta_2(s) = d_1 + \frac{c_1 s^{b_1}}{a_1^{b_1} + s^{b_1}}.$$

This function approximates the inverse of magnetic permeability of 4% Si steel. From the graph of $\beta_2(s)$ in Figure 4.1 one can see that the assumptions listed after (1.3) are satisfied. The concrete values are set to be $a_1 = 1.78,\ b_1 = 14,\ c_1 = 6000,\ d_1 = 245$.

Initially, all simulations featured oscillations of the zero level set. To stabilize the optimization process we introduce the Tikhonov regularization stabilizing term. We choose the squared norm of the gradient of the level set function. We use the coefficient α to control the trade-off between the fidelity term and the regularizing term. The cost function J from (1.5) thus obtains a new term resulting in

$$J(D) = \frac{1}{2}\int_D |\nabla u(\Omega) - \nabla m|^2 + \alpha \int_D |\nabla \phi|^2 \mathrm{d}x.$$

All the linear problems are solved on the regular triangular mesh with $2dim^2$ triangles constructed by splitting of the square into dim^2 small squares and next splitting each of them into two triangles.

We generate synthetic data using the model described in Section 1. This is to replace the real measurements with a nonlinear material. We set the following parameters $f = 5 \times 10^5,\ k = 40,\ dim = 30$.

The current density function f is a constant over the whole D. This setting generates a magnetic field with the strength between 0 and 2.7T.

5. Simulations. We present four simulations. In the first and second example we choose the exact domain to be a square in the middle of the domain. We perform two simulations with different initial guesses ϕ_0: one will be an ellipse located on the outside around the exact solution, see Figure 5.1(a), and second will be a circle crossing the exact solution, see Figure 5.2(a).

In the third and fourth example we choose exact domain as a triangle. Again we start simulations with two initial guesses, one will be an ellipse around the triangle and one will be a small allipse inside the triangle, see Figures 5.3(a) and 5.4(a).

The highest CPU time was attained by the fourth example. It took 132 minutes to run the simulation on a Intel® Core™2 Duo CPU P8600, 2.40GHz.

From Figure 5.1(a)–(f) we can see how the approximated void evolved. The initial shape has shrinked directly toward the exact solution. To reach the final state

it was necessary to run only 134 iterations. The regularization weight has been set $\alpha = 0.005$.

In Figure 5.2 is the situation different. The approximated shape has to transform from ellipsoidal shape to squared shape, then it has moved toward the exact solution, but one corner remained incorrect. And finally it filled the exact shape completely. The evolution was longer and to reach the final state it was necessary to run 1294 iterations.

To find out how the algorithm copes with sharper edges, we set the exact shape to be a triangle. In Figure 5.3 we can see that the lower corners of the exact solution have been captured directly and the approximated shape was accurate in these corners very fast. However the top corner of the triangle was difficult to capture. It took 877 iterations to converge to the exact solution.

Finally, in Figure 5.4 we see completely different behaviour, when evolving the approximated shape from the inside. In the beginning of the evolution process, the approximated shape just expanded, interestingly also over the borders of the exact shape. After a while the algorithm captured the exact shape and started to evolve in the right direction for all three corners. It took 1325 iterations to converge to the final state.

REFERENCES

[1] M. Brühl and M. Hanke. Recent progress in electrical impedance tomography. *Inverse Problems*, 19:65–90, 2003.

[2] J. Céa. Conception optimale ou identification de formes: calcul rapide de la dérivée directionnelle de la fonction coût. *RAIRO Modél. Math. Anal. Numér.*, 20(3):371–402, 1986.

[3] I. Cimrák. Inverse thermal imaging in materials with nonlinear conductivity by material and shape derivative method. *Mathematical Methods in the Applied Sciences*, 34:2303–2317, 2011.

[4] I. Cimrák and V. Melicher. Sensitivity analysis framework for micromagnetism with application to optimal shape design of magnetic random access memories. *Inverse Problems*, 23(2):563–588, 2007.

[5] I. Cimrák and V. Melicher. Determination of precession and dissipation parameters in the micromagnetism. *Journal of Computational and Applied Mathematics*, 234(7):2239–2249, 2010.

[6] I. Cimrák and R. Van Keer. Level set method for the inverse elliptic problem in nonlinear electromagnetism. *J. Comput. Phys.*, 229:9269–9283, 2010.

[7] S. Durand, I. Cimrák, and P. Sergeant. Adjoint variable method for time-harmonic Maxwell's equations. *COMPEL: The International Journal for Computation and Mathematics in Electrical and Electronic Engineering*, 28(5):1202–1215, 2009.

[8] J. Haslinger and P. Neittaanmäki. *Finite Element Approximation for Optimal Shape, Material and Topology Design*. Wiley, 2nd edition, 1996.

[9] F. Hettlich and W. Rundell. Identification of a discontinuous source in the heat equation. *Inverse Problems*, 17:1465–1482, 2001.

[10] K. Ito, K. Kunisch, and Z. Li. Level-set function approach to an inverse interface problem. *Inverse Problems*, 17(5):1225–1242, 2001.

[11] S. Osher and R. Fedkiw. *Level Set Methods and Dynamic Implicit Surfaces*, volume 153 of *Applied Mathematical Sciences*. Springer-Verlag, New York, 2003.

[12] H.M. Park and H.J. Shin. Shape identification for natural convection problems using the adjoint variable method. *Journal of Computational Physics*, 186(1):198 – 211, 2003.

[13] V. Ya. Rivkind and N. N. Ural'tseva. Classical solvability and linear schemes for the approximate solution of the diffraction problem for quasilinear equations of parabolic and elliptic type. *Journal of Mathematical Sciences*, 1(2):235–264, 1973.

[14] P. Sergeant, I. Cimrák, V. Melicher, L. Dupré, and R. Van Keer. Adjoint variable method for the study of combined active and passive magnetic shielding. *Mathematical Problems In Engineering*, 2008:15 pages, 2008.

[15] J. Sokołowski and J. P. Zolésio. *Introduction to shape optimization*, volume 16 of *Springer*

Series in Computational Mathematics. Springer-Verlag, Berlin, 1992. Shape sensitivity analysis.

[16] X. Zhang. Uniqueness of weak solution for nonlinear elliptic equations in divergence form. *International Journal of Mathematics and Mathematical Sciences*, 23(5):313–318, 2000.

[17] J. P. Zolésio. The material derivative (or speed) method for shape optimization. In *Optimization of distributed parameter structures, Vol. II (Iowa City, Iowa, 1980)*, volume 50 of *NATO Adv. Study Inst. Ser. E: Appl. Sci.*, pages 1089–1151. Nijhoff, The Hague, 1981.

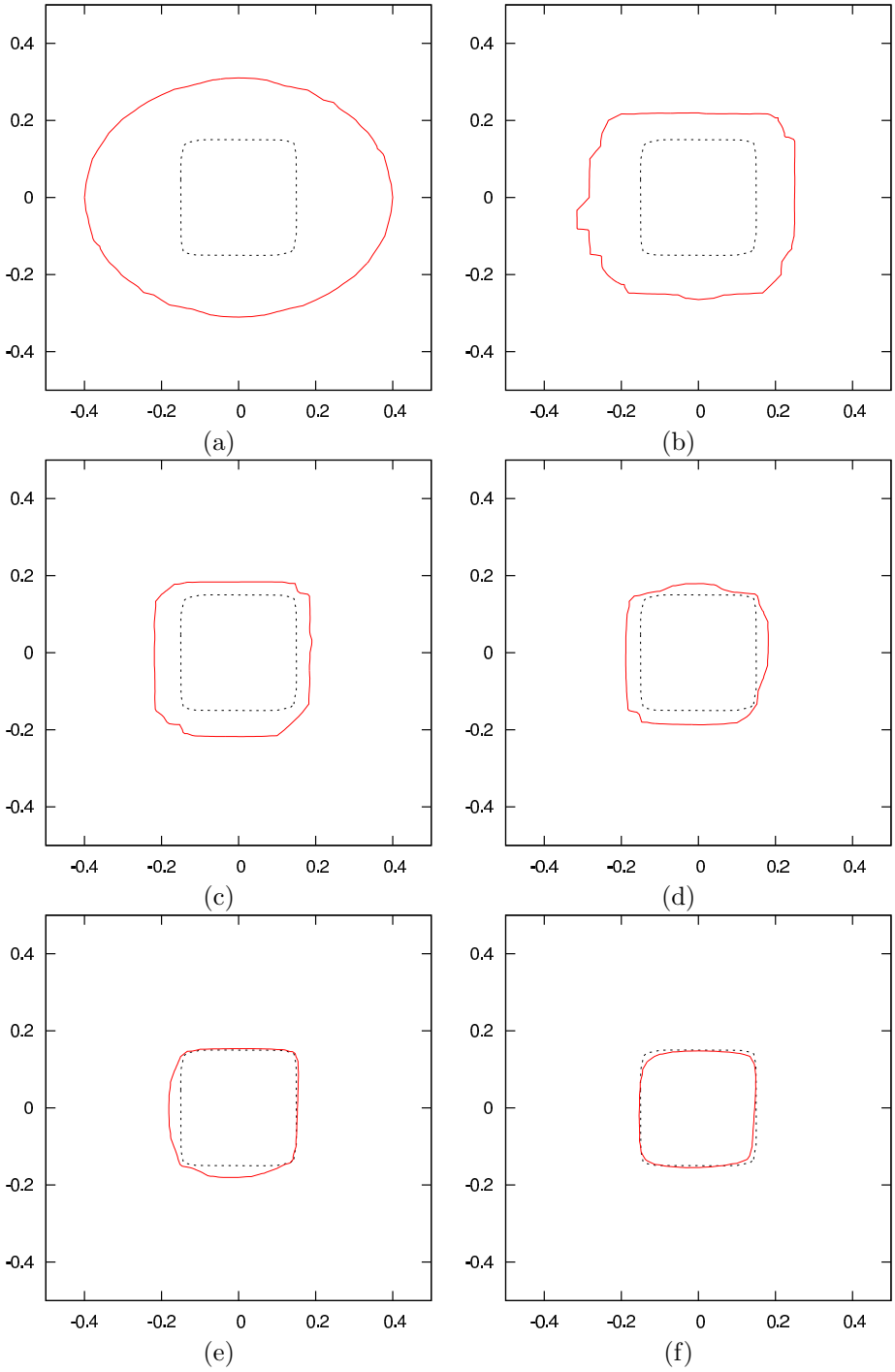

FIG. 5.1. *(a) The exact D_{ex} consists of a square in the middle and is plotted with the black dashed line. The initial guess is a large ellipse outside the exact shape, and is plotted with the red solid line. (b) The approximation represented by the zero level set of ϕ after 12 iterations. (c) Evolution of the zero level set after 29 iterations, (d) after 48 iterations, (e) after 75 iterations, and (f) after 134 iterations.*

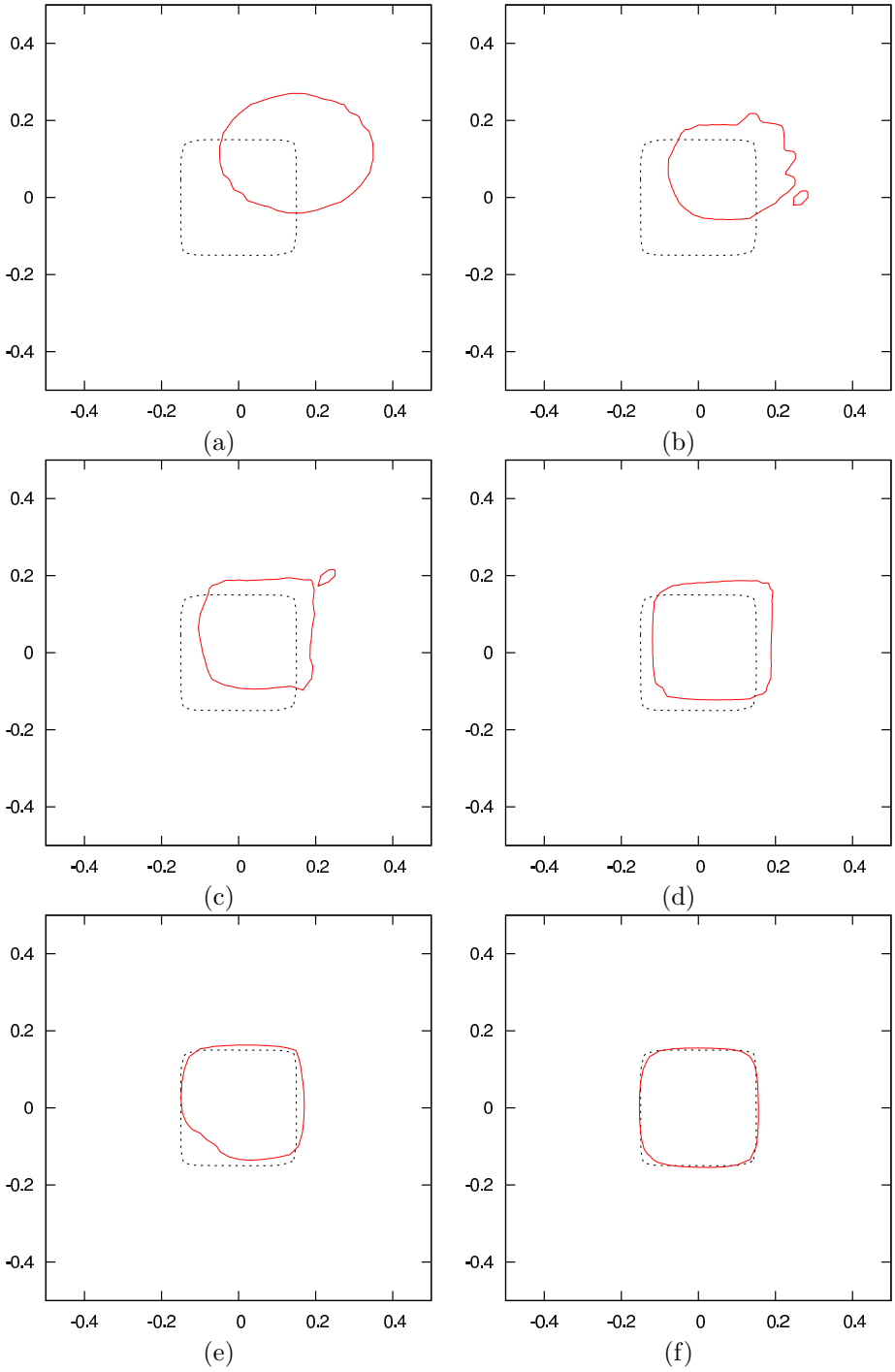

FIG. 5.2. *(a) The exact D_{ex} consists of a square in the middle and is plotted with the black dashed line. The initial guess is a circle crossing the boundary of the exact shape, and is plotted with the red solid line. (b) The approximation represented by the zero level set of ϕ after three iterations. (c) Evolution of the zero level set after 16 iterations, (d) after 48 iterations, (e) after 501 iterations, and (f) after 1294 iterations.*

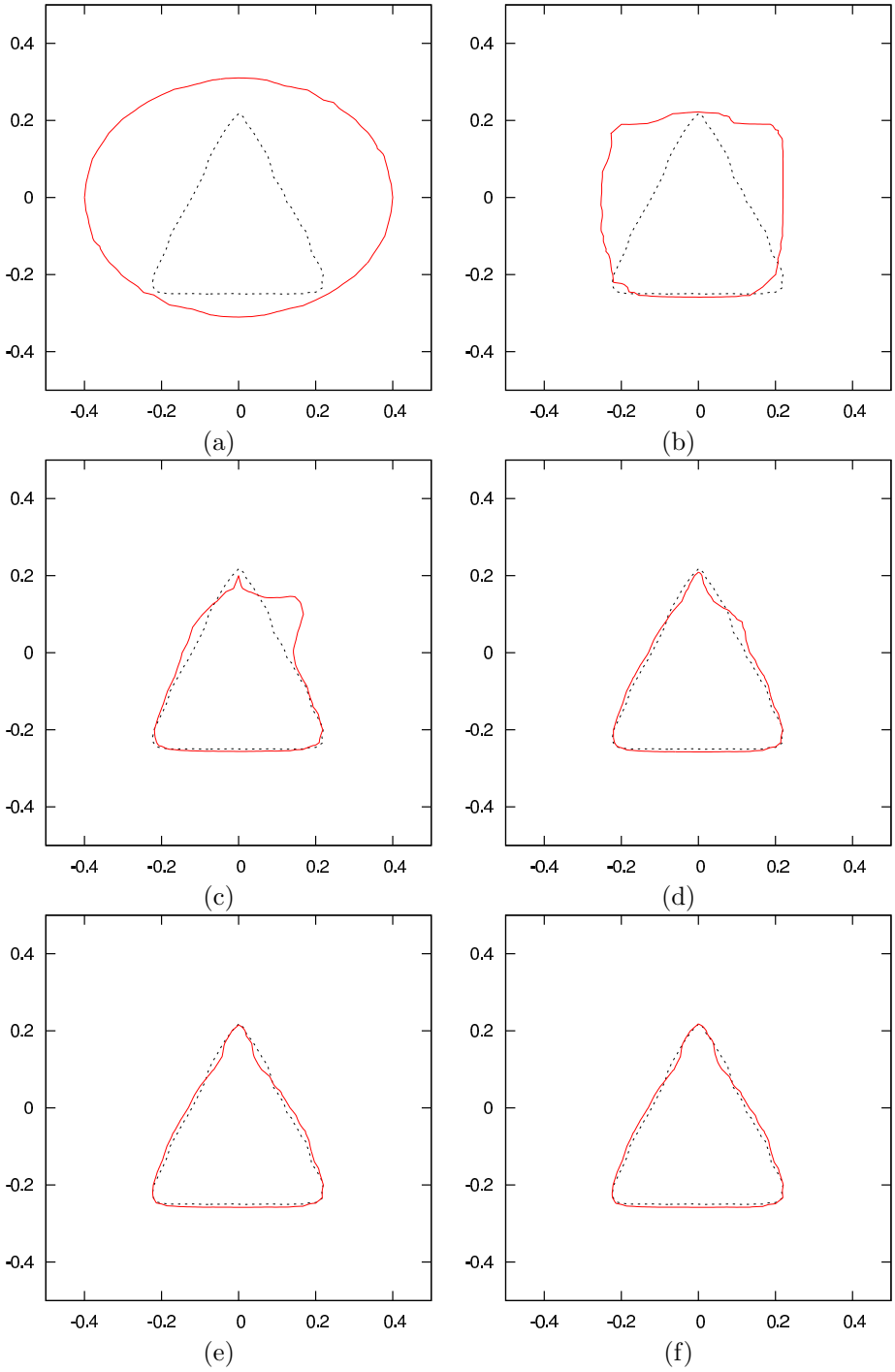

FIG. 5.3. *(a) The exact D_{ex} consists of a triangle in the middle and is plotted with the black dashed line. The initial guess is a large ellipse outside the exact shape, and is plotted with the red solid line. (b) The approximation represented by the zero level set of ϕ after 31 iterations. (c) Evolution of the zero level set after 199 iterations, (d) after 284 iterations, (e) after 462 iterations, and (f) after 877 iterations.*

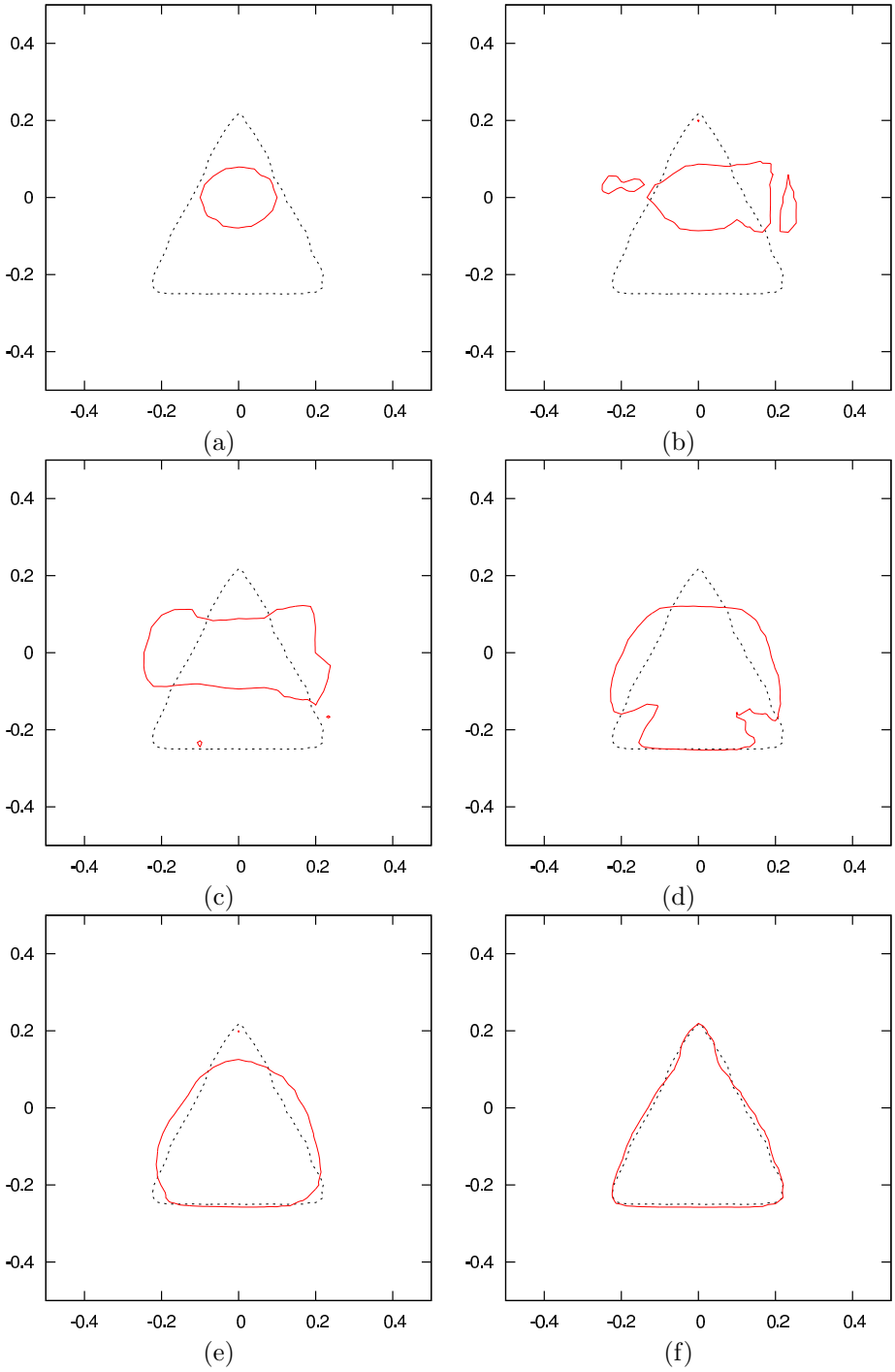

FIG. 5.4. *(a) The exact D_{ex} consists of a triangle in the middle and is plotted with the black dashed line. The initial guess is a small ellipse inside the exact shape, and is plotted with the red solid line. (b) The approximation represented by the zero level set of ϕ after four iterations. (c) Evolution of the zero level set after 27 iterations, (d) after 236 iterations, (e) after 349 iterations, and (f) after 1325 iterations.*